CHAPTER III

PARENT MCM-41 SYNTHESIS AND CHARACTERIZATIONS

3.1 Introduction

Since 1992, the discovery of a new family of mesoporous molecular sieves, M41S aroused worldwide studies in this field [Beck, 1992]. MCM-41 is one member of the M41S family, which possesses a regular hexagonal array of uniform pore openings. The MCM-41 molecular sieve has been investigated extensively because the other members in this family are either thermally unstable or difficult to obtain. This attractive material has prompted new opportunities for applications in catalysis, chemical separation, adsorption media and advanced composite materials [Zhao, 1996]. Unfortunately, MCM-41 has not yet been commercialized, so it is necessary to prepare MCM-41 materials for further comparison work.

This chapter presents a comprehensive overview of MCM-41 synthesis, by means of common preparation technique at room temperature and atmospheric pressure as well as its proposed formation mechanisms. The studies of the effect of synthesis parameters such as aging time and pH are also discussed. The basically physical characterizations for porous solids i.e., distinctive crystallinity, functional groups determination and surface property analysis including surface area, pore size distribution, pore diameter are performed. The physical properties of MCM-41 are then evaluated by comparing it with what has been that found in the literatures.

3.2 Objectives

The synthesis of the MCM-41 prototype and its characterization were described in this chapter. The main objectives were listed below.

1. To synthesize siliceous MCM-41 material as a controlled sample following the method reported elsewhere. In consideration of the MCM-41 preparation, the reasonable procedure was introduced.
2. To examine typically physical characteristics of the mesoporous solid and chemical compositions of the synthesized MCM-41 material. The comparison of all properties of the sample and the MCM-41 found in references were also illustrated.

3.3 Literature Review

3.3.1 Molecular Sieve Materials

Porous solids are used technically as adsorbents, catalysts and catalyst supports depending to their surface properties. According to the International Union of Pure and Applied Chemistry (IUPAC) definition, porous materials can be classified into three groups: macropores with diameters greater than 500 Å, mesopores with diameters between 20 and 500 Å, and micropores with diameters less than 20 Å. The various molecular sieves generally found in the applications of materials and catalysis chemistry has been ordered by the determination based on pore diameter as presented in Table 3-1.

Table 3-1 Pore size distribution of various molecular sieves [Zhao et al, 1996].

Pore size (Å)	Definition	Typical material	Pore diameter (Å)
>500	Macroporous		>100
20-500	Mesoporous	MCM-41	15-100
<20	Microporous	Zeolite	<15
	Ultra-large pores	Cloverite	6.0 x 13.2
		JDF-20	6.2 x 14.5
		$AlPO_4$-8	7.9 x 8.77
	Large pores	Faujasite	7.4
		$AlPO_5$-5	7.3
	Medium pore	ZSM-12	5.5 x 5.9
		ZSM-48	5.3 x 5.6
		ZSM-5	5.3 x 5.6
	Small pore	CaA	4.2
		SAPO-34	4.3

At present, porous materials have played an important role in catalysis. They exhibit outstanding properties such as large surface area and high adsorption capacity, of which hydrophobicity or hydrophilicity can be tailored by tuning carbon chain length of surfactants and controlling synthesis factors. Furthermore, the channel openings and cavities are in the ranges of many interests. The unique pore structure makes the materials able to recognize molecules and facilitate the selectivity of reactions, transition states and products within those pores. This may be used to direct processes towards desired products. Consequently, large pore crystalline materials are not applicable in catalytic processes even though large pore material has been made. Today the most promising materials in the microporous and mesoporous ranges seem to be more attractive.

Well-known members of the microporous series are zeolites, crystalline silica compounds synthesized from a complex of amorphous silica and inorganic materials. The self-assembly of polymerized $[SiO_4]^{4-}$ and $[AlO_4]^{5-}$ provides the condensation of silicate ion structuring in aluminosilicates networks. The various coordination types of zeolite are found as Faujasite X and Y, ZSM-5, ZSM-12 and ZSM-22. Zeolites have been greatly expanded in the interests for the uses as adsorbents and excellent materials for catalytic reaction within industrial areas dedicated to oil refining, petrochemistry, synthesis of chemicals and environmental applications. However, their applications are limited due to their small pore opening which is unachievable with the large kinetic diameter of some reactants [Jen, 2000].

In 1988, Yanagisawa et al. reported the syntheses of ordered mesoporous materials with narrow pore size distributions and large surface areas. The materials were prepared from the layered polysilicate named kanemite. First the Na ions in the kanemite interlayers are ion-exchanged by alkyltrimethyl ammonium cations. Second, the flexible kanemite layers fold and cross-link to each other and in this way an inorganic framework is formed. The driving force of this rearrangement is assumed to be the structural loss of kanemite and the ability of the surfactants to transform from bilayer structures to cylindrical micellar aggregates. The silicate species rearrange further around the micelles and silanol condensation finally forms an inorganic network.

In 1992, researchers at the Mobil Research and Development Corporation reported the first successful synthesis of the M41S family of silicate/aluminosilicate mesoporous molecular sieve with excellent uniform pore structure and narrow pore size distribution in the range of 15 and 100 Å [Beck et al., 1992]. The new concept of the synthesis proposed is the use of self-assembled surfactants such as cetyltrimethyl ammonium (CTA) cation as a molecule template rather than the conventional single-templated zeolite. M41S have been grouped into four catagories, as seen in Figure 3-1. Two have been identified as the thermally stable: MCM-48 displaying a three-dimensional, cubic-ordered pore structure and MCM-41 having a one-dimensional, hexagonally-ordered pore structure. The two other unstable phases are lamellar MCM-50 and molecular octamer.

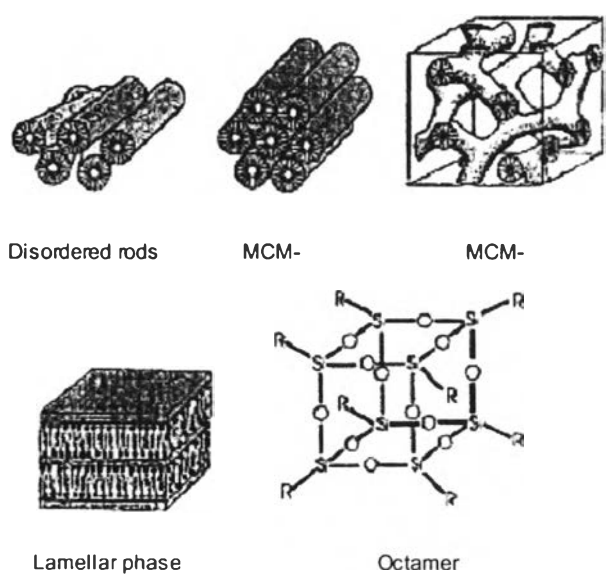

Figure 3-1 Phase formation of MCM family obtained from CTAB/SiO_2/water [Selvam et al., 2001].

All of these phases provide well-defined XRD patterns. Figure 3-2 illustrates the typical diffraction pattern along with the disordered forms. These materials are fundamentally different from zeolites by the fact that their pore walls are amorphous and pore sizes are larger in the mesoporous range [Zhao et al., 1996]. The functional groups analyses of MCM-41 molecular sieve are carried out by Infrared spectroscopy. Figure 3-3 shows the FTIR spectrum of the calcined samples compared to amorphous

silica. Three absorption peaks identical to amorphous silica are observed, whereas the peak near 961 $cm^{-1}$is particularly observed in the MCM-41 material.

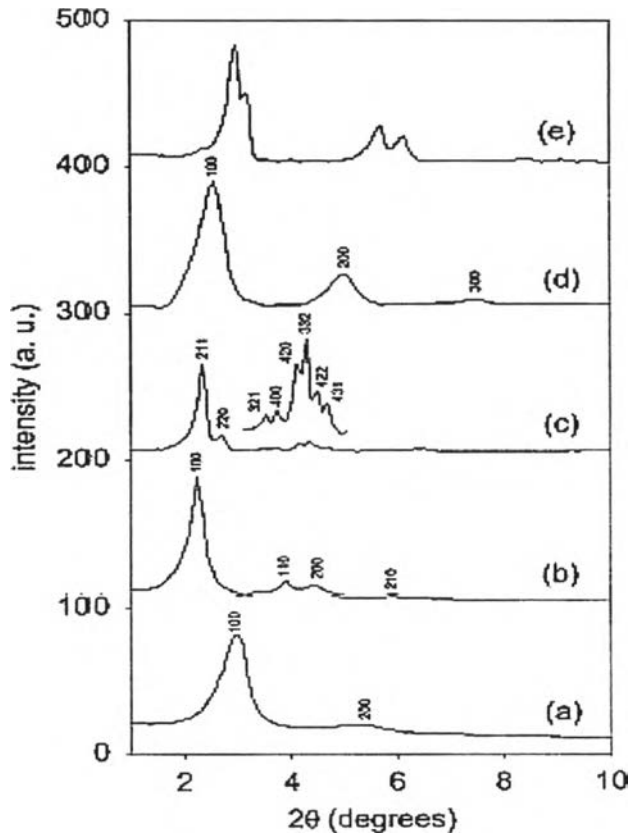

Figure 3-2 Powder X-ray diffraction patterns of (a) disordered MCM-41, (b) ordered MCM-41, (c) MCM-48, (d) MCM-50 and (e) Octamer [Selvam et al., 2001].

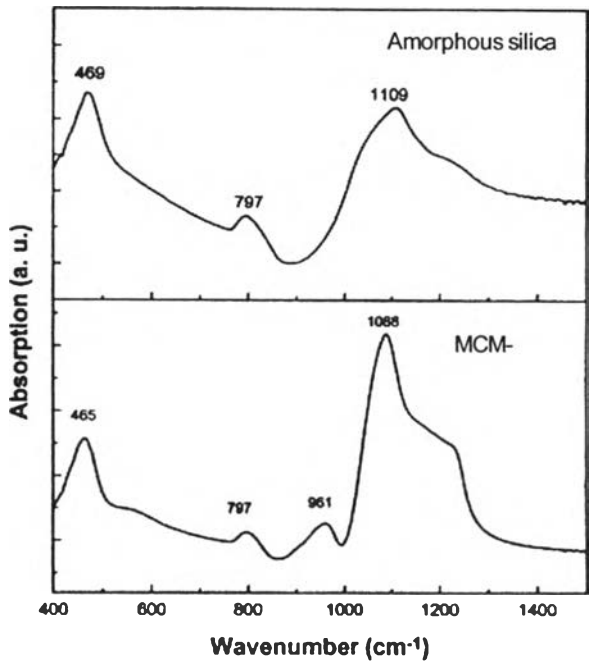

Figure 3-3 FTIR spectra of MCM-41 molecular sieve and amorphous silica [Gu, 1999].

MCM-41, one of the M41S family, has attracted worldwide interest in many areas of physical, chemical, and engineering sciences. This is because of its structural simplicity and ease in preparation with negligible pore-networking and pore-blocking effects. MCM-41 has also been identified as the most suitable model of mesoporous adsorbent presently available for the adsorption studies. The prominent features of siliceous MCM-41, and in general of most mesoporous materials are as follows: well-defined pore shapes (hexagonal/cylindrical); narrow distribution of pore size; very high degree of pore ordering; tailoring and fine-tuning of the pore dimensions (1.5-50 nm); large pore volumes (> 0.6 cm^3 g^{-1}); exceptional sorption capacity (64 wt% of benzene at 50 Torr and 25 °C); very high surface area (700-1500 m^2 g^{-1}); hydrophobic and mild acidic surface, high surface reactivity; ease of modification of the surface properties, and excellent thermal, hydrothermal, chemical, and mechanically stability.

The excellent properties of MCM-41 are conducive for a number of important applications such as adsorption, separation, ion exchange, catalysis, and molecular hosts. In the past few years, the expansion of the activities and scientific research for this versatile material has been witnessed. One of interesting advantages for MCM-41

has recently been performed in environmental research. Conversion of fly ash into M41S type materials, membrane, chromatography, electron-transfer materials, and sorption of heavy metals and volatile organic substances have been developed. Due to stringent environmental regulations, heterogeneous catalysis, other alternative for environmental application, offers simple separation, easy recovery, reuse, waste reduction, and elimination of hazardous chemicals, in addition to their uses in both gas and liquid phase operations. However, the limitation of siliceous MCM-41 in catalytic process is its neutral framework. Without any chemical modification, it has greatly utility as adsorbents, molecular sieves, and supports. For advance in the variety of catalysis, it needs to be modified by the incorporation of heteroions into the silicate framework to promote its capability. Recently, the heterogeneous catalytic reactions such as hydrogenation, hydrocracking, hydrodesulfurization, hydrodenitrogenation, hydrodehalogenation, nitric oxide reduction, carbon monoxide oxidation and polymerization reactions have been established.

3.3.1.1 Synthesis of Siliceous MCM-41 Molecular Sieve

The original MCM-41 synthesis was carried out in water under alkaline solution similar to zeolite. The four main components in the MCM-41 syntheses are structure-directing surfactants, a source of silica, a solvent and a catalyst, an acid, or a base. In their pioneering work on the M41S materials, the Mobil researchers used alkyltrimethyl ammonium halides as the structure-directing surfactants and combinations of sodium silicate, tetraethylorthosilicate (TEOS) and fumed silica (anhydrous amorphous silica) as the silica source. In the cases of aluminosilicate materials, an aluminum source was added as well.

Low molecular weight surfactants, $C_nH_{2n+1}(CH_3)_3N^+$ (n=8-22) or $C_nH_{2n+1}C_5H_5N^+$ (n = 12 or 16) which have a hydrophilic (water-soluble) headgroup and a hydrophobic (water-insoluble) tail group were employed as structure-directing agents. In general, the surfactants with 12, 14, and 16 carbon atoms give good MCM-41 properties because micelle packing, a major parameter of material crystallinity, is suitably controlled. The high-molecular-weight surfactants ($\geq C_{18}$) are difficult to dissolve and rarely used. On the other hand, the lower-molecular-weight surfactants

($\leq C_{10}$) seem to have different in forms the self-assembled shape which provides less order materials with broad pore size distribution. The different pore sizes of MCM-41 (2-5 nm) can also be controlled by varying the alkyl chain length. Larger pore diameter can be obtained by using large-head-group cationic surfactants.

The stabilized binary mixture was produced as by the following procedure. The silica source is hydrolyzed and condensed to form multicharged anions that can coordinate with the surfactant headgroups. The silica species and the surfactant assemble into a silica-surfactant phase, and a gel network is formed. It was noticed that the formation of stable MCM-41 is also affected by the reactivity of the ingredients used in synthesis. For example, sodium silicate is more reactive than fumed amorphous silica [Chen, 1993]. Then, the binary mixture under constant stirring was aged at certain temperatures for 24-144 h depending on the method used. Chen also found that the shorter synthesis time can be obtained by increasing synthesis temperature. The pH of the synthesis gel was then adjusted in the range of 8-11 using a mineral acid or base such as sodium hydroxide or ammonium hydroxide. After crystallization in an aging period, the silicate ions were condensed to form a siloxane framework and the solid products were filtered, washed with deionized water and dried. Finally, the materials were calcined at 550 °C under gas flow (nitrogen, oxygen, or air) to remove the organic template [Beck, 1992]. Selvam (2001) also reported that depending on the actual synthesis strategies such as hydrothermal, microwave or ambient synthesis, the precipitate can typically be obtained from room temperature up to 150 °C in few minutes to several days. After calcinations, the white bulky solid containing hexagonally porous structures were produced. Transmittion Electron Microscope (TEM) image seen in Figure 3-4 displays the well-defined honey comb structure, a unique characteristic of MCM-41 material prepared from C_6 orthosilicate. However, it was evident that methods for surfactant removal by calcinations affect the surface area, pore size, and pore volume of material. The alternative template extractions including acid treatment, oxygen plasma treatment, liquid phase extraction and supercritical fluid extraction have been employed. In case of solvent extraction, acid, ethanol, ammonium acetate, and a mixture of ethanol and ammonium acetate are commonly used. The solvent extracted MCM-41 has a larger pore size than the calcined sample.

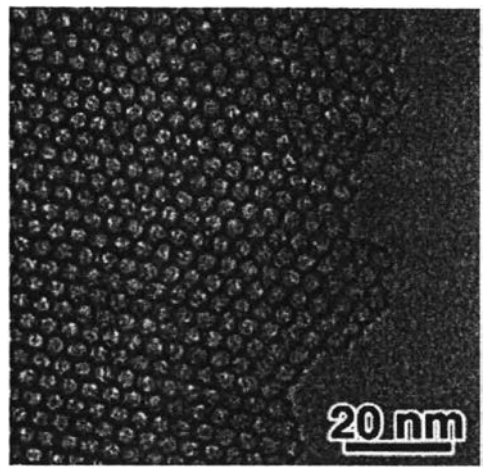

Figure 3-4 High resolution TEM images of calcined MCM-41 [Jaroniec et al., 2001].

Ryoo and Kim (1995) proposed the synthesis of a highly crystallized MCM-41 by mixing alkyltrimethylammonium bromide with sodium silicate (11.3 wt% Na_2SiO_4 and 88.6 wt% H_2O) at room temperature. The pH of the mixture which was initially heated to 100 °C for 1 day was adjusted at 10 by the addition of 30 wt % of acetic acid following by heating as before. The latter procedure was repeated twice before solid filtration. Another study of the effect of various acid and pH adjustments on MCM-41 structure was conducted by Edler and White (1997). This was achieved with sulfuric acid and a pH in the range of 9-10. By means of recommended procedures, the highly ordered MCM-41 with narrow pore size distribution was obtained.

Chen and Wang (2002) introduced another route for the synthesis of MCM-41, containing complementary textural porosity and high thermal stability. The difference compared to Rayoo and Kim was the change in the silica source. Instead of using sodium silicate, tetraethyl orthosilicate (TEOS) was employed as a reactive silicate precursor. The gel was prepared by a mixture of CTAB and TEOS with the optimum surfactant/ silicon molar ratio of 0.10. They also found that an increase of TEOS content in the initial gel resulted in a material which is no longer mesoporous due to the production of the excess ethanol from the hydrolysis and condensation of TEOS. Likewise, Kumar (2001) proposed the novel synthesis of MCM-41 at room temperature with high resistivity to hydrolysis by using CTAB and TEOS with the molar ratio 1 M TEOS: 12.5 M NH_4OH: 54 M EtOH: 0.4 M CTAB: 174 M H_2O.

The thermal and hydrothermal stability of MCM-41 were improved by decreasing the number of silanol groups in the framework structure. Igarashi et al. (1999) found that the low hydrothermal stability in water of MCM-41 was due to the hydrolysis of siloxane bonds in the presence of adsorbed water even in air saturated with moisture. Increasing the hydrophobicity by decreasing the silanol groups was introduced for the enhancement of hydrothermal stability. The removal of silanol groups can be done by postsynthesis treatment with acid, modification by silylation and ion exchange with alumina.

The Mobil researchers also found that the relative concentrations of the species present in the synthesis solutions were the great importance for the final pore structures. The pore diameter of MCM-41 increases as the chain length of the surfactant increases. This brought about the modification of synthesis methods by improving the long-range structure of MCM-41. Furthermore, the optimum pH value for the synthesis gel and surfactant/silicate ratio are found to be main parameters related to the structural appearance of MCM-41. The effects of these two synthesis parameters were reviewed as shown below.

3.3.1.1.1 Effect of Surfactants/Silicate Ratio

As mentioned above, a mixture of n-alkyltrimethylammonium and n-alkyltriethylammonium surfactant cations (n = 12-22) are commonly used for ordered MCM-41 preparation. In a simple binary system of water-surfactant, surfactant molecules act as very active components affecting the first stage formation of ionic template. With increasing concentration, surfactant molecules aggregate together to form micelles in order to decrease the system entropy. The initial concentration threshold at which monatomic molecules aggregate to form isotropic micelles is called *cmc* (critical micellization concentration).

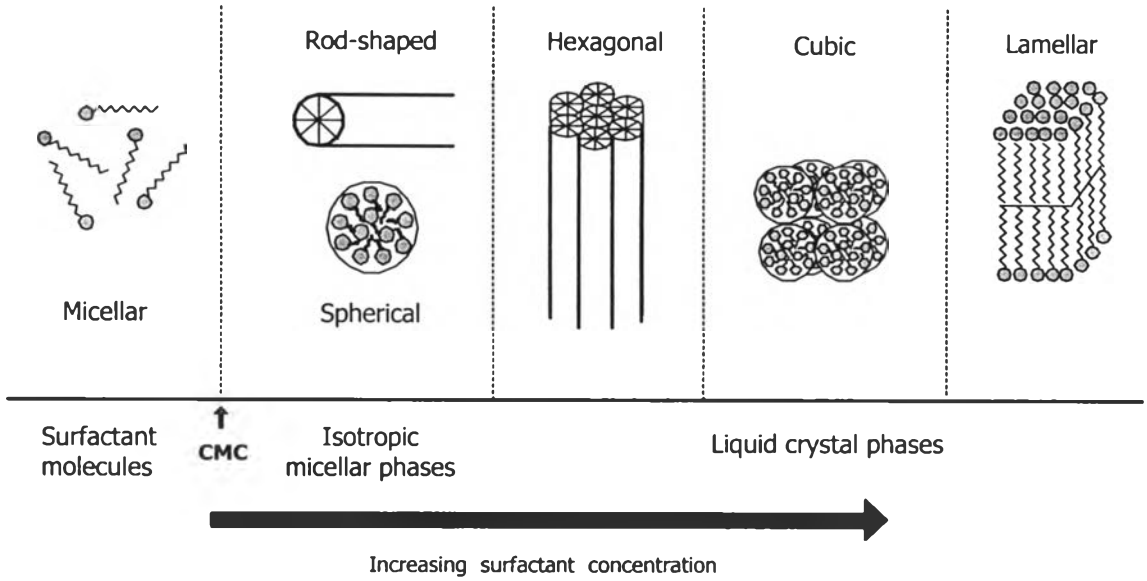

Figure 3-5 Phase sequence of surfactant and water binary system adapted from Zhao [1996].

Figure 3-5 presents the phase sequence of the surfactant and water binary system. As the concentration process continues, hexagonal close packed arrays appear, producing the hexagonal phases. The next step in the process is the coalescence of the adjacent, mutually parallel cylinders to produce the lamellar phase. The cubic phase is generally believed to consist of complex, interwoven networks of spherical aggregates.

The particular phase in a surfactant aqueous solution depends not only on the concentrations but also on the nature of itself (the length of the hydrophobic carbon chain, hydrophilic head group, and counterion) and the environmental parameters (pH, temperature, its ionic strength, and other additives). Generally, the cmc decreases with the increase of the chain length of a surfactant, the valency of the counterions, and the ion strength in a solution, respectively. On the other hand, it increases with increasing counterion radius, pH, and temperature.

For example, in an aqueous solution at 25 °C, the cmc is about 0.83 mM for surfactant $C_{16}H_{33}(CH_3)_3N^+ Br^-$; between the cmc and 11 wt %, small spherical micelles are present; in the concentration range of 11-20.5 wt %, elongated flexible rodlike micelles are formed [Chen et al., 1993]; hexagonal liquid crystal phases appear in the concentration region between 26 and 65 wt %, followed by the

formation of cubic, lamellar, and reverse phases with increasing concentration [Lawrence, 1994]. As the temperature increases, the required concentration for a sphere-to-rod transformation increases as well. At 90 °C, the hexagonal phase is observed at a surfactant concentration of more than 65% [Steel, 1994].

3.3.1.1.2 Effect of Synthesis pH

Another parameter that influences the crystallinity and quality of MCM-41 is the pH of the synthesis gel, as well as the nature of pH adjustment. The immediate pH adjustment results in poorly crystallized structure of MCM-41. On the other hand, the gradual adjustment of pH prolongs the surfactant molecules and silicate species assembling together to form more ordered molecular structures.

There are various silicate structures found in an alkaline solution so far. These silicate species are important for the formation of surfactant template of zeolite and molecular sieve synthesis. It has been found that the distribution of these anionic silicate species is sensitive to pH, temperature, cation, and Si concentration. A reduction in silicon concentration or increase in temperature or pH favors the formation of monomer and small oligomers. This various kinds of silicate species provide the alternative templates for the reaction of other anionic counterions such as monomeric $Al(OH)^-_4$ (the only species in alkaline solution with pH 7-13) which is the predominant aluminosilicate template for zeolite and molecular sieve synthesis.

3.3.1.2 Formation and Mechanisms of MCM-41 Synthesis

The outstanding mechanism of MCM-41 preparation is different from the traditional single molecules templating in zeolite synthesis in that the templates are not single organic molecules but long chain surfactants, having an alkyl chain length more than 6 carbons (in most case greater than 10 carbons). Since the discovery of the MCM series, their several pathway formations and mechanisms have been proposed. From the reviews up to the present, the most well known mechanism, suggested by Beck et al. (1992) is 'liquid crystal templating' or the LCT mechanism. The formations of inorganic and organic species are based on electrostatic interactions

between the positive charges of surfactants and negative inorganic ions. In the model from Figure 3-6, two possible reaction pathways were proposed:

Pathway 1. The liquid-crystal phase occurs before silicate ions are added.

Pathway 2. The prior addition of silicate species affects the ordering of self-assembly of that surfactant micelle.

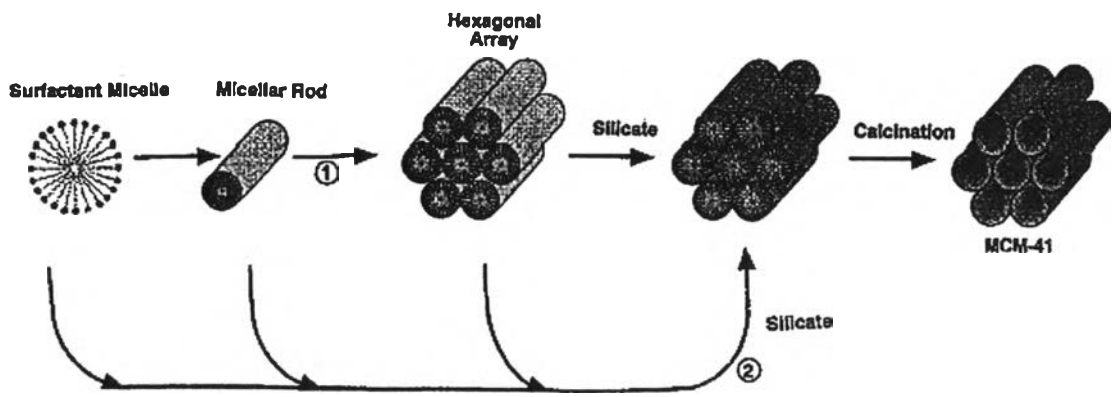

Figure 3-6 Possible mechanistic pathways for the formation of MCM-41: (1) liquid crystal phase, (2) silicate anion [Beck et al., 1992].

The distinct feature of the LCT mechanism (pathway 1) is that the liquid crystalline mesophases or micelles act as templates connecting together like a preformed hexagonal array. The final product is a silicate skeleton that contains many voids inside after the organic templates are removed. Thus, the silicate condensation is not a predominant factor in the performance of mesophase. According to the LCT mechanism, the pore size is directly dependent on how existing liquid crystal micelles are completely formed.

The influences of alkyl chain length and aging temperature on LCT formation were investigated by Beck et al. (1992). An increase of chain length greatly improves the subsequence of amorphous phase in the order from poorly ordered MCM-41 to well performed MCM-41. On the contrary, on increase of aging temperature contributes to the abatement in degree of crystallization, causing poor pore size distribution and disarranged mesophase.

In 1993, Chen et al. suggested another MCM-41 mechanism different from that previously proposed. The results from XRD, in situ ^{29}Si NMR and thermogravimetric analysis insistently defined the model of silicate anions (pathway 2). No hexagonal LCT was detected either in the synthesis gel or in the surfactant solution. The majority of mechanism was that the randomly rod-like micelles individually interact with silicate species in the optimal reaction mixture to produce two or three monolayers of silicate encapsulation. Then, these random silicate cylinders spontaneously pack into a highly ordered mesoporous material. However, in order to produce highly ordered hexagonal structures, large amounts of surfactant generally more than 10 wt % of total mixture, were required. It can be believed that liquid crystal micelles still exist in the mixture; therefore, the LCT mechanism seems to be more acceptable.

The differences of these reaction pathways result from the change of surfactant properties such as alkyl chain length and the strength of cationic charge. Similarly, concentration of surfactant and pH affects the critical micelle concentration (CMC) in prepared solution. Beck also suggested that in very dilute aqueous solution ($\sim 10^{-3}$ to 10^{-2} mol L^{-1} surfactant concentration), the existing species are spherical not rod-like micelle as was proposed previously.

3.3.2 Gas Phase Adsorption Theory

Physical adsorption or physisorption is an adsorption which is recognized to occur at the surfaces of solids is due to van der Waals forces such as those that exist between molecules themselves, including electrostatic attraction in the case of molecules with permanent dipole moments and induced dipolar attraction. In general, physisorption occurs only at temperatures close to the boiling point of the adsorbate at the operative pressure and its strength relate to the physical properties of the adsorbing species; in other words, the strength depends very little on the chemical nature of solids. Unlikely, chemical adsorption or chemisorption involved the rearrangement of the electrons of the interacting gas and solid with formation and destruction of chemical bonds [Thomas, 1996]. Chemisorption and physisorption are usually distinguishable from each other by means of enthalpy of adsorption, which is

the heat liberated when a mole of a substance is transferred from the gaseous to the adsorbed state, activation energy, reaction temperature and number of layers adsorbed as summarized in Table 3-2 [Bond, 1987].

Table 3-2 Criteria for distinguishing between chemisorption and physisorption.

Criterion	**Physisorption**	**Chemisorption**
Enthalpy of adsorption (- H_{ads})	8-20 kJ mol^{-1}	40-800 kJ mol^{-1}
Activation energy (E_a)	Zero	Usually small
Temperature of occurrence	Depends on boiling point, but usually low	Depends on E but usually low
Number of layers adsorbed	More than one possible	Not more than one

Adsorption is usually exothermic because it is a spontaneously occurring process, ΔG is negative or ΔH-$T\Delta S$ must also be negative. Now ΔS will also be negative because adsorption produces a more ordered system with fewer degrees of freedom so, ΔH must be negative which means the exothermic process.

3.3.2.1 Classification of Isotherms and Hysteresis Types

The characterization of porous adsorbents and catalysts has become a large field of research in the scientific community. The surface areas of both internal and external surfaces, as well as the total pore volume, are typically determined using the physical adsorption of a gas. It is now known that there are two types of adsorption, chemical adsorption (chemisorption) and physical adsorption (physisorption). Some of the characteristic differences between these are: 1) chemisorption involves large heats of adsorption, typically on the order of a chemical reaction, while physisorption involves relatively small heats of adsorption; 2) physical adsorption is readily reversible, whereas chemical adsorption requires large energies to break the bonds formed; and 3) chemically adsorbed species are limited to a monolayer of coverage, whereas physical adsorption can form in multiple layers.

Many porous solids exhibit isotherm hysteresis where the desorption isotherm does not follow the adsorption isotherm. The hysteresis occurs when the desorption of the adsorbate from mesopores takes place at a pressure lower than that of capillary condensation. In general, hysteresis attributes to the different sizes of the pore mouths and pore bodies or to the different adsorption and desorption behaviors in near-cylindrical pores. Sing (1989) classified types of hysteresis loops into four patterns presented in Figure 3-7. The hysteresis associated with specific isotherm is a physical property supporting the characteristic of each different porous solid. There are six types of isotherms of gases on solids, as recognized by IUPAC (Barton et al., 1999), and these are shown in Figure 3-8. The first five were classified by Brunauer et al. (1940) and sub-classes of Type I, II, and IV isotherms are demonstrated in Figure 3-9 [Rouquerol et al., 1999].

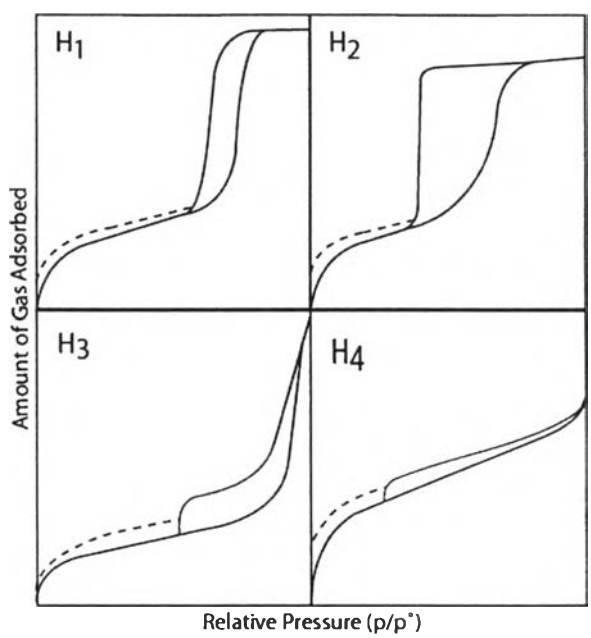

Figure 3-7 Types of hysteresis classified by Sing (1989).

Type H_1 hysteresis loops, in which the adsorption and desorption branches of the loop are nearly vertical and almost parallel to each other, are found in solids having nearly uniform size pores and a narrow PSD. Type H_2 hysteresis is broader than Type H_1, with the desorption branch being steeper than the adsorption branch of the loop. This type of hysteresis is indicative of complex, interconnected networks of

pores with varying sizes and shapes. Type H_3 hysteresis is found in particles with non-rigid, slit-shaped pores. Type H_4 hysteresis is common in adsorbents with slit-shaped pores primarily in the micropore range. The closure point of the hysteresis loop is dependent on the adsorptive and the operational temperature, and is represented by the dashed lines in Figure 3-7.

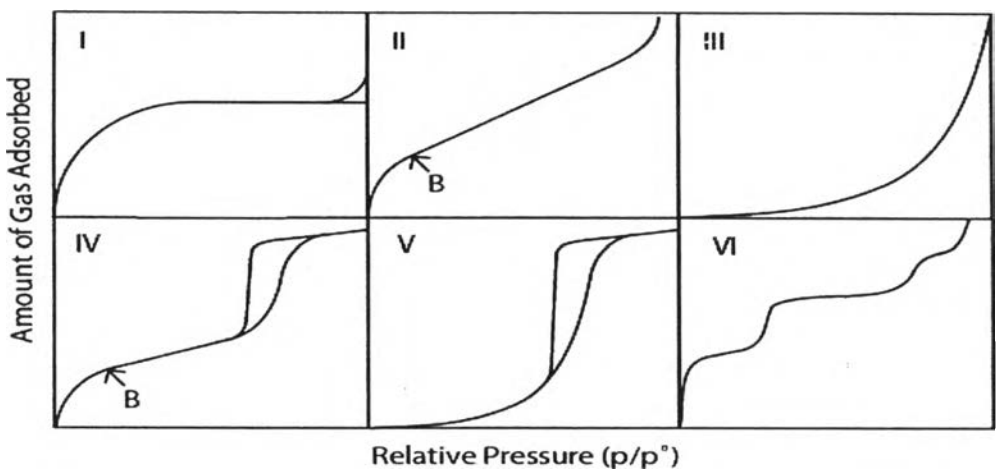

Figure 3-8 IUPAC classification of adsorption isotherms.

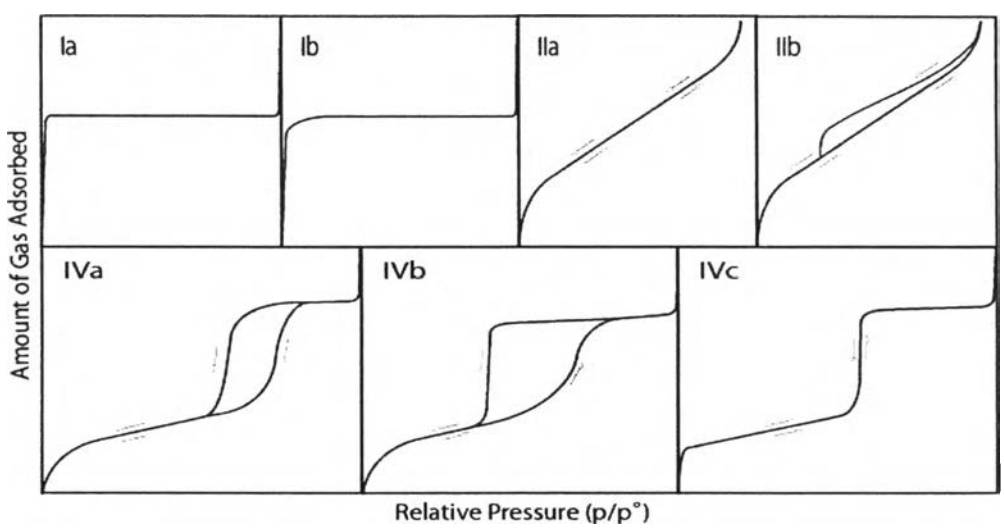

Figure 3-9 Sub-classification of isotherms.

Type I isotherms, originally defined by Langmuir indicates a relatively small amount of multilayer adsorption leading to a small external surface area. The sub-class of Type I are Ia and Ib when the primary micropore filling takes place in pores at very low relative pressures and cooperative micropore filling takes place in wider

ones at slightly higher relative pressures, respectively. Type I isotherms are not commonly found in practical adsorbents.

Type II isotherms can either be reversible (IIa) or exhibit a Type H_3 hysteresis loop (IIb). The reversible Type II isotherm is typically attributed to monolayer formation followed by multilayer formation. Solids exhibiting a Type IIa isotherm can be non-porous, macroporous, or possibly even microporous. Type II isotherms are commonly encountered in industrial adsorbents.

Type III isotherms are also associated with monolayer-multilayer adsorption; however, the adsorbent-adsorbate interactions are weak when compared to adsorbate-adsorbate interactions. Type III isotherms with the hysteresis loop typically associated with capillary condensation is identified as Type V isotherms. Type III and V isotherms are relatively uncommon.

Type IVa and IVb isotherms are commonly found in inorganic oxide xerogels and other porous solids. The difference being that multilayer coverage is complete at some pressure below the saturation vapor pressure and reflect the phenomenon of capillary condensation. Type IVa isotherms exhibit Type H_1 hysteresis, while type IVb isotherms demonstrate Type H_2 hysteresis. Type IVc isotherms are found in specially prepared silicas, e.g., MCM-41 type materials, and represent a reversible isotherm with a steep vertical section, which occurs in materials with a narrow range of uniform, cylindrical pores. With certain qualifications, it is possible to analyze Type IV isotherms by means of Nitrogen 77 K in order to obtain a reasonable estimate of the specific surface and an assessment of the pore size distribution.

A Type VI isotherm is typically found during adsorption of a simple non-polar gas on a uniform surface such as graphite. The steps represent a layer-by-layer adsorption process onto the solid.

3.3.2.2 A Model System for Adsorption Studies on Mesoporous Materials

In 1911, Zsigmondy theorized that vapors can condense in small pores, now known as mesopores, and current theory of capillary condensation is based largely on

this theory [Rouquerol et al., 1999, Gregg & Sing, 1982]. Zsigmondy advanced studies by Lord Kelvin; based on thermodynamic principles that the equilibrium vapor pressure over a concave meniscus of liquid is less than that of the saturation vapor pressure. When a vapor condenses on a flat surface, a mechanical equilibrium exists between the vapor and liquid phases. In order to maintain this equilibrium on a flat surface in a constant temperature system, the pressure of the gas (p gas), the saturated vapor pressure (p_0) and the pressure of the liquid (p liq) must all be equal. In a capillary, the adsorption layers in the pores form a concave liquid-gas interface (meniscus). Compared to the vapor pressure at the liquid-gas interface of a flat surface, the pressure of gas over a concave surface is less than the saturated vapor pressure (p gas $< p_0$). This leads to vapor condensation in pores at pressures less than p_0, a phenomenon which Zsigmondy called *capillary condensation* [Gregg & Sing, 1982]. In porous solids it is widely accepted that capillary condensation is responsible for the filling of mesopores. Capillary condensation follows the process of multilayer adsorption, and the pores become liquid filled.

The Kelvin equation, the advanced studies of Zsigmondy theory in 1911 relates this reduced pressure (p/p_o) to the radius of curvature of a concave meniscus as shown in (Equation 3-1). This theory is based on thermodynamic considerations of free energy change, and is used to calculate the pore size distribution (PSD) of a solid (Gregg & Sing, 1982).

$$\ln\left(\frac{p}{p_0}\right) = \frac{-2\gamma V_L}{r_m RT} \qquad \textbf{(3-1)}$$

Here p/p_0 is the relative pressure of vapor in equilibrium with a meniscus having a radius of curvature r_m, and γ and V_L as the surface tension and molar volume of the liquid adsorptive, respectively.

In the years 1916-1918, Langmuir developed his theory of adsorption based on a kinetic model, and it is still widely recognized today as a pioneering effort in the characterization of solids [Gregg & Sing, 1982]. This theory is based on the concept

of an array of active sites on the surface of the adsorbent, to which one molecule can adsorb onto each site, interactive forces exist between molecules, and only a monolayer film formed along the flat surface [Langmuir, 1918]. The Langmuir adsorption isotherm shows a linear relationship between the amount adsorbed and the pressure of the adsorbate. Clearly, this method does not represent adsorption on practical porous adsorbents and is very rarely used to determine the surface area of adsorbents.

In the1940s, Brunauer, Emmett and Teller published the BET theory which has been widely used for the determination of porous solid structures using gas adsorption. Today, it is standard practice to measure the physical adsorption of nitrogen at 77 K, and the data are typically evaluated using the BET method corrected for the film thickness (Sing, 2001). The assumptions underlying the simplest BET isotherm are as follows:

- Gas adsorbs on a flat, uniform surface of the solid with a uniform heat of adsorption due to Van der Waals forces between the gas and the solid.
- There is no lateral interaction between the adsorbed molecules.
- After the surface has become partially covered by adsorbed gas molecules, additional gas can adsorb either on the remaining free surface or on top of the already adsorbed layer. The adsorption of the second and subsequent layers occurs with a heat of adsorption equal to the heat of liquefaction of the gas.

Even though this theory was reliable on the assumption mentioned above, the disadvantage of the BET theory has been determined. It is now known that forces between the adsorbate molecules, as well as the forces exerted by the pore walls, affect the surface tension and density of the liquid within the pores. The doubtable explanation of the BET theory has directed researchers toward finding corrected values of surface tension and density when evaluating adsorption data. Although, the BET model has been questionable due to significant limitation in its usage, this theory remains the most popular method for surface area calculations today. Attempts have been made by many researchers [Brunauer and Deming, 1940, Brunauer Teller, 1938] to modify the BET equation using more fitting parameters and have resulted in a modified Kelvin equation.

In 1951, Barrett, Joyner, and Halenda (BJH) published a method for estimating the volume and area of porous adsorbents. By assuming cylindrical pores, zero contact angle and correcting for the thickness of the layer already adsorbed, the radius of each pore (r_p) can be calculated using the sum of the Kelvin radius (r_k) and the thickness of the film (t) at that relative pressure as illustrated in Equation 3-2 and Figure 3-10.

$$r_p = r_k + t \quad \text{.....(3-2)}$$

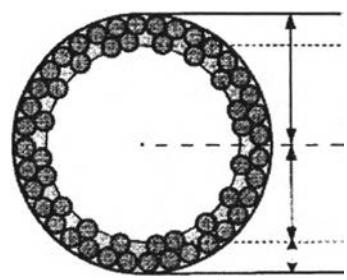

Figure 3-10 Pore and core models for mesoporous adsorbent adapted from Naono (2001).

The Kelvin equation modified for a cylindrical porous solid is presented in Equation 3-3. With this equation, Pore Size Distribution (PSD) can be calculated by using the adsorption or desorption isotherm information.

$$\ln\left(\frac{p}{p_0}\right) = \frac{-\sigma V_L}{r_k RT} \quad \text{.....(3-3)}$$

where σ is the surface tension of the bulk adsorbate at system temperature. In the case of desorption process, the meniscus of the condensed adsorbate was usually assumed to be hemispherical and the following form of the Kelvin equation was obtained:

$$r_k = \frac{4.078}{\ln\left(\frac{p}{p_0}\right)} \quad \text{.....(3-4)}$$

When $\gamma = 8.88$ mN m^{-1}, $V_L = 34.68$ cm^3 mol^{-1} at 77 K

The adsorptions were transformed into *t-plot* by replacing the relative pressure (p/p_o) into the statistical thickness (t) of the adsorbed layer at the corresponding relative pressure. The relationship of wall thickness (t) obtaining from the BET plot could be revealed as the following equation, which was used later in order to compute the pore diameter (Rouquerol, 1999).

$$t = 3.54\left(\frac{-5}{\ln\frac{P}{p_0}}\right)^{0.333} \quad \text{.....(3-5)}$$

Many authors have reported that BET measurements and PSD analysis using the BJH equation (Equation 3-2 and 3-3) may underestimate the pore volume in porous solids, and should only be used as a first approximation (Sing, 1989; Carrott et al., 2001). This is because the thickness of the multilayer formation is assumed to be in a close-packed liquid-like state when using the BET approach. It is believed that the molecules within the pore spaces may be in a much more tightly bound state, leading to surface areas for the molecules smaller than on a flat plate, hence, underestimating the pore volume.

3.4 Experimental

In this chapter, MCM-41 called *Parent MCM-41* was chemically produced from a commercial silica source. In order to produce a good quality of MCM-41 product that is both cost-effective and environmentally friendly, the most empirically promising route without pre- and post-synthetic treatment was introduced.

3.4.1 Materials and Chemicals

- Hexadecyltrimethylammonium bromide, CTAB (Wako Pure Chemical Industries, Ltd.)
- Tetraethylorthosilicate, TEOS (98%, Aldrich)
- Ammonium hydroxide (29.80 %, Carlo Erba)
- Ethanol (99.8 %, Carlo Erba)
- Deionized water
- Air zero

3.4.2 Apparatus and Instruments

- Teflon beaker
- Quartz tube (5 cm. diameter and 50 cm. length)
- Furnace
- X-Ray Diffractometer (Bruker model axs D5005 X-diffraction)
- Fourier Transform Infrared spectrometer (Nicolet: model Impact400D)
- Transmission Electron Microscope (JEOL-JEM-200 CX)
- Scanning Electron Microscope (JEOL-JSM-6400)
- Micromeritics Sorption Analyzer (ASAP 2010)

3.4.3 Methodology

Since MCM-41 has not been yet commercialized, the parent MCM-41 was synthesized by the method modified from Kumar (2001). The reaction easily took place at room temperature under atmospheric conditions. CTAB and TEOS were used as a commercial surfactant and silica source respectively. To moderately produce 1 g of MCM-41, the amount of those reactant was prepared in the molar basis of 0.15

CTAB: 1 TEOS: 1.64 NH_4OH: 1.26 H_2O. The exhaustive procedure is presented below.

1. One g of CTAB was dissolved in 50 mL of deionized water in the Teflon beaker and vigorously stirred until the solution was homogeneous and clear.
2. 3.33 mL of 1 M ammonium hydroxide was added slowly into the solution. Then, the mixture was stirred further for 5 minutes at room temperature.
3. After that, 4.162 mL of TEOS was transferred into the aqueous solution. The homogeneous mixture was stirred continuously at room temperature for 2 days to allow for the crystallization.
4. Then, the gel was filtered through Whatman paper No. 48 using vacuum suction, rinsed with 30 mL of ethanol and washed with deionized water consecutively.
5. The precipitated solid was calcined at 550 °C in the furnace purged with air for 5 h. Finally, it was cooled and kept in desiccator.

3.4.4 Sample Characterizations

The physical structure and properties of calcined samples were examined by spectroscopic and microscopic techniques. The study of crystallinity change was carried out by XRD diffractogram. Physical characteristics of the sample, in particular the specific surface area, pore size, pore volume and pore sized distribution was determined by Nitrogen adsorption isotherms combined with the BET method. FTIR spectroscopy provided the descriptions of functional groups contained in MCM-41. In addition, material features, morphology and molecular arrangement were examined by the SEM and TEM microscopic techniques. The sample preparations and analysis condition are described later.

3.4.4.1 X-Ray Diffraction (XRD)

Powder XRD patterns were obtained using Cu Kα radiation on a Bruker axs D5005 diffractometer. The x-ray was generated with a current of 40 mA and a

potential of 40 kV. The samples were scanned from 1 to 10 degrees (2θ) in steps of 0.06 degrees per minute. The powder patterns of the samples were recorded at the same time and with the same amount of material, so that the intensity of the peak height (100) could be compared.

3.4.4.2 Scanning Electron Microscope (SEM)

Sample powder was sprinkled as a thin layer on adhesive tape on a brass bar. Excess amount was blown away with an air spray. The sample was then coated with gold in the JEOL (JFC-1100E Ion) sputtering device and transferred into the JEOL (JSM-6400) sample chamber at the accelerating voltage of 15-40 kV.

3.4.4.3 Transmission Electron Microscope (TEM)

Prepared specimens were deposited on a 300 mesh copper grid and rapidly transferred to a JEOL-JEM-200 CX transmission electron microscope operated at 100 kV.

3.4.4.4 Fourier Transform Infrared Spectrometry (FTIR)

The sample was ground with an agate mortar and pestle until it was approximately the same consistency as the KBr powder then added and mixed thoroughly with the mixture. After that the homogeneous powder was transferred into sample barrel and pressed with 13 tons force for 1 minute and put on a V-mount cell. The FTIR spectrum was recorded in the range of 400-4000 cm^{-1}.

3.4.4.5 Nitrogen Adsorption Isotherms and Brunauer, Emmett and Teller (BET) Analysis

The adsorption and desorption isotherm and surface area were measured at 77 K on a Micromeritics ASAP 2010 sorption analyzer using nitrogen. Before measurement, samples were pretreated with heat at 105 °C over night to remove moisture then outgassed at room temperature under the vacuum. The t-plots shapes are identical to those of α-plots determined from the N_2 adsorption isotherm. Specific

surface areas of the studied materials were calculated using the standard BET method at the relative pressure range of 0.05-0.15. Pore diameters were estimated from the peak positions of BJH pore size distribution curves calculated from the adsorption isotherms. The mesoporous volumes were estimated from the amount adsorbed at the relative pressure of about 0.95.

3.4.5 Results and Discussion

3.4.5.1 XRD Characteristics

The XRD patterns of the calcined parent MCM-41 typically exhibits four reflections corresponding to Bragg peaks in the range of 2θ between 2-8 at 2.6, 4.2, 4.8, and 6.3 as seen in Figure 3-11. The reflections are due to the ordered hexagonal array of parallel silica tubes and can be indexed assuming a diffraction unit cell as (*d100*), (*d110*), (*d200*) and (*d210*), which are distinctive patterns particularly found in pure silica MCM-41 [Beck, 1992; Chen, 1993; Ciesla, 1999]. The high intensity of *(d100)* spacing illustrates the hexagonal mesoporous material with a high degree of long range ordering of the structure and well-formed hexagonal array presented in the parent sample.

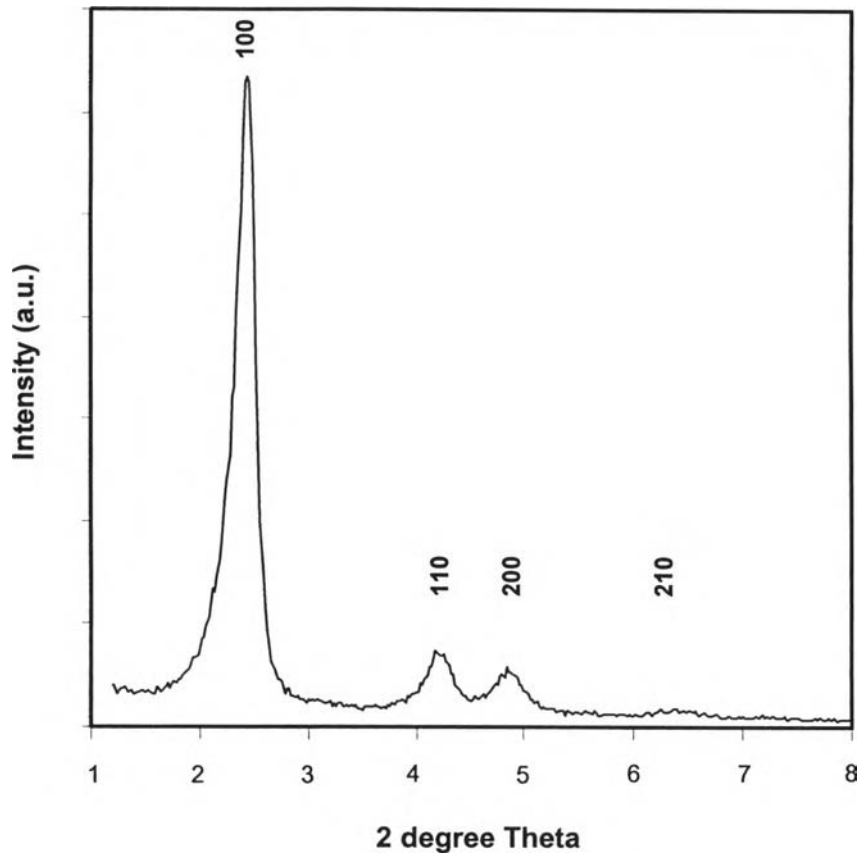

Figure 3-11 X-ray powder diffraction patterns of the parent MCM-41.

3.4.5.2 Nitrogen Isotherms and BET Analysis

Although the XRD crystallinity pattern was found to correspond to the reference peak of MCM-41, the surface analysis of the surface area, pore volume, pore diameter and pore size distribution was required for proper characterization of porous solid. The specific surface area can be obtained from nitrogen isotherms using the BET model (Equation 3-7). By means of nitrogen isotherms, the pore size distribution, pore diameter and pore wall thickness can be calculated by using the BJH method described in Equation 3-2 to 3-4.

The nitrogen adsorption and desorption isotherms for the parent MCM-41 materials are shown in Figure 3-12. The step in the isotherms reflects a narrow and uniform distribution of the pore size, while its height indicates the pore volume. According to IUPAC classification, the typical sorption measurements follow the type

IVc isotherm with a high porosity (0.87 $cm^3 g^{-1}$) and a large surface area (800 ± 25 $m^2 g^{-1}$). This type IVc isotherm is a characteristic of porous materials with a narrow range of uniform and cylindrical pores. At low relative pressures (P/P_0 < 0.26), the formation of a monolayer of adsorbed molecules is the predominant process. At higher pressures (P/P_0 > 0.26), the adsorption in mesopores leads to multilayer formation until condensation takes place, giving a sharp increase in adsorption volume. As the mesopores are filled, the adsorption continues on the external surface. The isotherms usually exhibit a sharp inflection at P/P_0 in a range of 0.30-0.40, corresponding to capillary condensation within uniform mesopores. The sharpness of this step inferred the uniformity of pore size distribution. The information revealed from the nitrogen isotherms is a unique characteristic found in good agreement with mesoporous materials reported elsewhere [Selvam, 2001; Zhao, 1996].

Small significant hysteresis identified as Type H_1 hysteresis was observed in the adsorption and desorption isotherms. The Type H_1 hysteresis loops inferred that the synthesized MCM-41 was a mesoporous solid having nearly uniform size pores or a narrow pore size distribution.

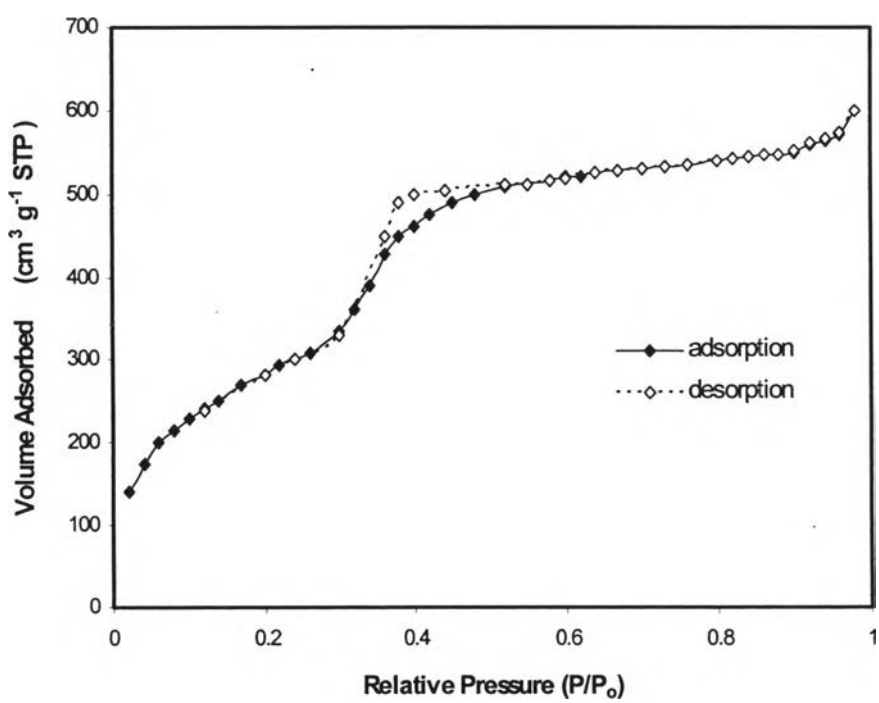

Figure 3-12 Adsorption (solid line) and desorption (dotted line) isotherms of nitrogen at 77 K on the parent MCM-41.

The plot of the derivative of the specific pore volume (V) with respect to the pore diameter (D) as (dV/dlogD) versus the pore diameter is shown in Figure 3-13. The calculation was based on the BJH method, which is basically used for the physisorption of nitrogen on a porous solid. It was found that the pore size distribution was quite narrow, and in the range of 20-35 Å. As shown in Figure 3-13, the average pore diameter determined from the adsorption isotherm was 29.5 Å and that from the desorption isotherm was 29.0 Å.

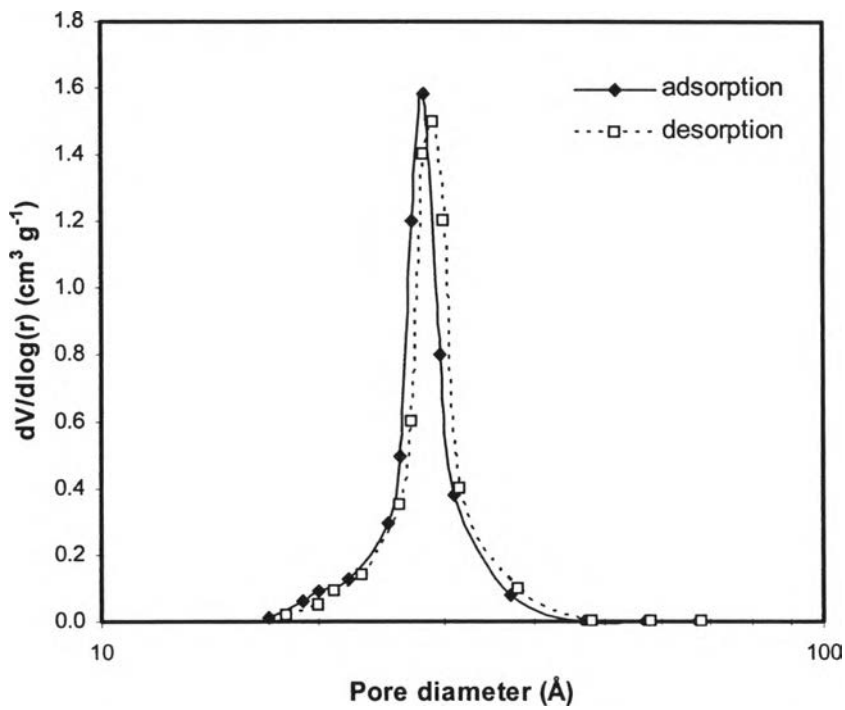

Figure 3-13 Pore size distributions of the parent MCM-41 calculated from nitrogen adsorption and desorption isotherms at 77 K by using BJH model.

3.4.5.3 SEM Morphology

Surface morphology of the synthesized sample was characterized using the SEM technique. The SEM image shown in Figure 3-14 could not show details of the pore wall structure due to the inadequate magnitude and resolution of scanning. However, it was seen that two kinds of agglomerated crystals, circled-like and drum-like particles with particle size estimated in the range of 500-1000 nm were observed.

These morphologies were similar to the SEM results of highly ordered MCM-41 [Cai et. al., 1999]. The details of hexagonal pore structure were determined by using the TEM technique which is described later.

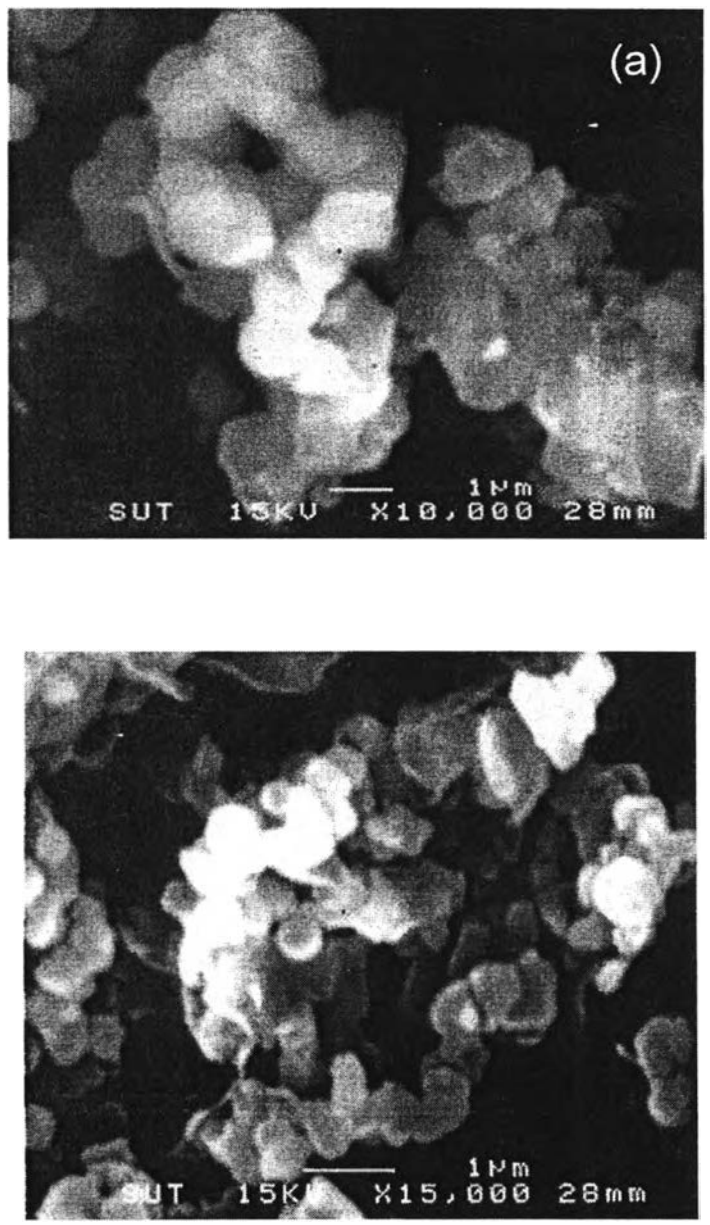

Figure 3-14 SEM images of the parent MCM-41 with the magnitude 10,000x (a) and the magnitude 15,000x (b).

3.4.5.4 TEM Morphology

To elucidate the pore structure of MCM-41, Transmission Electron Microscopy (TEM) was used. Figure 3-15 shows a TEM image of the hexagonal arrangement of uniform, approximately 3 nm-sized pores in a sample of MCM-41. Because of the limitation of image resolution, the exact analysis of pore sizes and thickness of the pore walls are very difficult and not possible without additional analysis. The wall thickness can be determined by using the nitrogen adsorption data as mentioned above. However, it should be noted that pores of MCM-41 are likely to be hexagonal rather than circular. The formation of the hexagonal pore walls was already explained in terms of maintaining the self-assembled rod like structure which is discussed later.

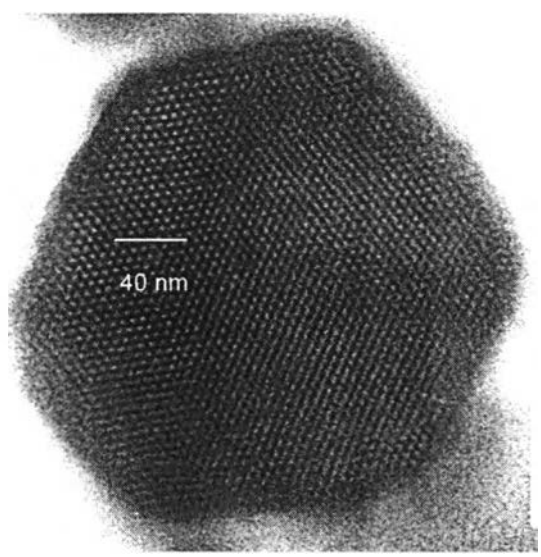

Figure 3-15 TEM image of the parent MCM-41 with the magnitude of 150,000x.

3.4.5.5 Fourier Transform Infrared Spectrometry (FTIR)

Infrared spectrometry is applied to the qualitative and quantitative determination of molecule species of all types. The most widely used region is the mid-infrared that extends from about 400 to 4000 cm^{-1}. The well-known transmittance spectra of the parent MCM-41 are visible in Figure 3-16. The vibrational mode 480 cm^{1} is represented as Si-O bonds. A peak exhibited near 800 cm^{-1} is attributed to the

symmetrical Si-O-Si stretching mode. High intensity contributed at 1100 cm^{-1} is due to the vibration of oxygen atoms joining with the adjacent silicon atoms in the asymmetric stretching of Si-O-Si bonds. A broad absorption around 3500 cm^{-1} is due to H-bonded silanols (Si-OH), which acts as proton acceptors. It was obviously seen that the main FTIR peaks of the MCM-41 particles shows a characteristic of amorphous silicon dioxide (SiO_2), which is similar to the pattern found in rice husk silica. The additional peak appeared around 961 cm^{-1}, which is assigned to the symmetric stretching vibration of Si-OH groups and identified to be a distinguished appearance of the MCM-41 molecular sieve [Gu, 1999]. The interfering spectrum at 1600 cm^{-1} is inferred as the presence of carbon dioxide generally associated in the sample.

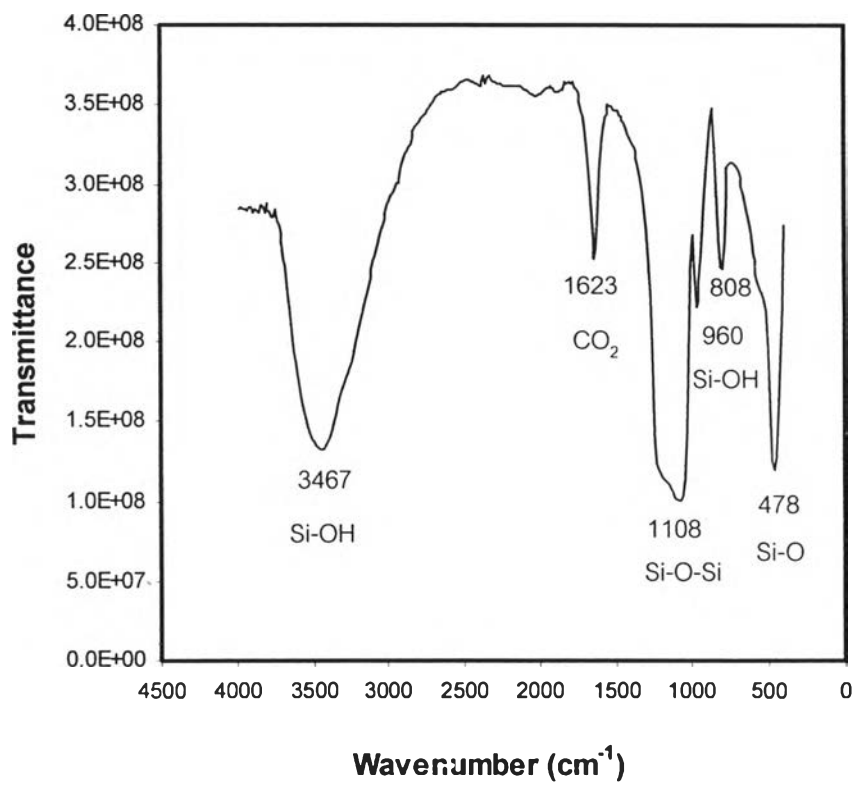

Figure 3-16 Transmittances FTIR spectra of the parent MCM-41.

3.4.5.6 Formation Mechanism of MCM-41

The schematic diagram of MCM-41 formation is presented in Figure 3-17. As proposed by many authors, the properties of MCM-41 are significantly influenced by

reactants, synthesis parameters and the method used. In this work, the parent MCM-41 was prepared by using CTAB and TEOS in the aqueous solution at 25 °C. The mechanism was described as follows. The CTAB molecules are first protonated to be highly reactive CTA^+, which later forms rod-like micelles, while TEOS molecules are hydrolyzed and form negative silicate species. The formation of a liquid crystal phase is performed initially one by one single rod by the deposit of silicate species on the organic templates to produce the silicate walls of MCM-41. In concentrated solution, many nuclei are formed, and grow in the early stage, followed by aggregation of these nuclei to form hexagonal arrays. After nucleation growth, the calcination is employed consequently to remove the template out and stabilize the pore structure. The final product is siliceous MCM-41, which possesses a uniformly hexagonal structure and contains functional groups corresponding to the characterization results.

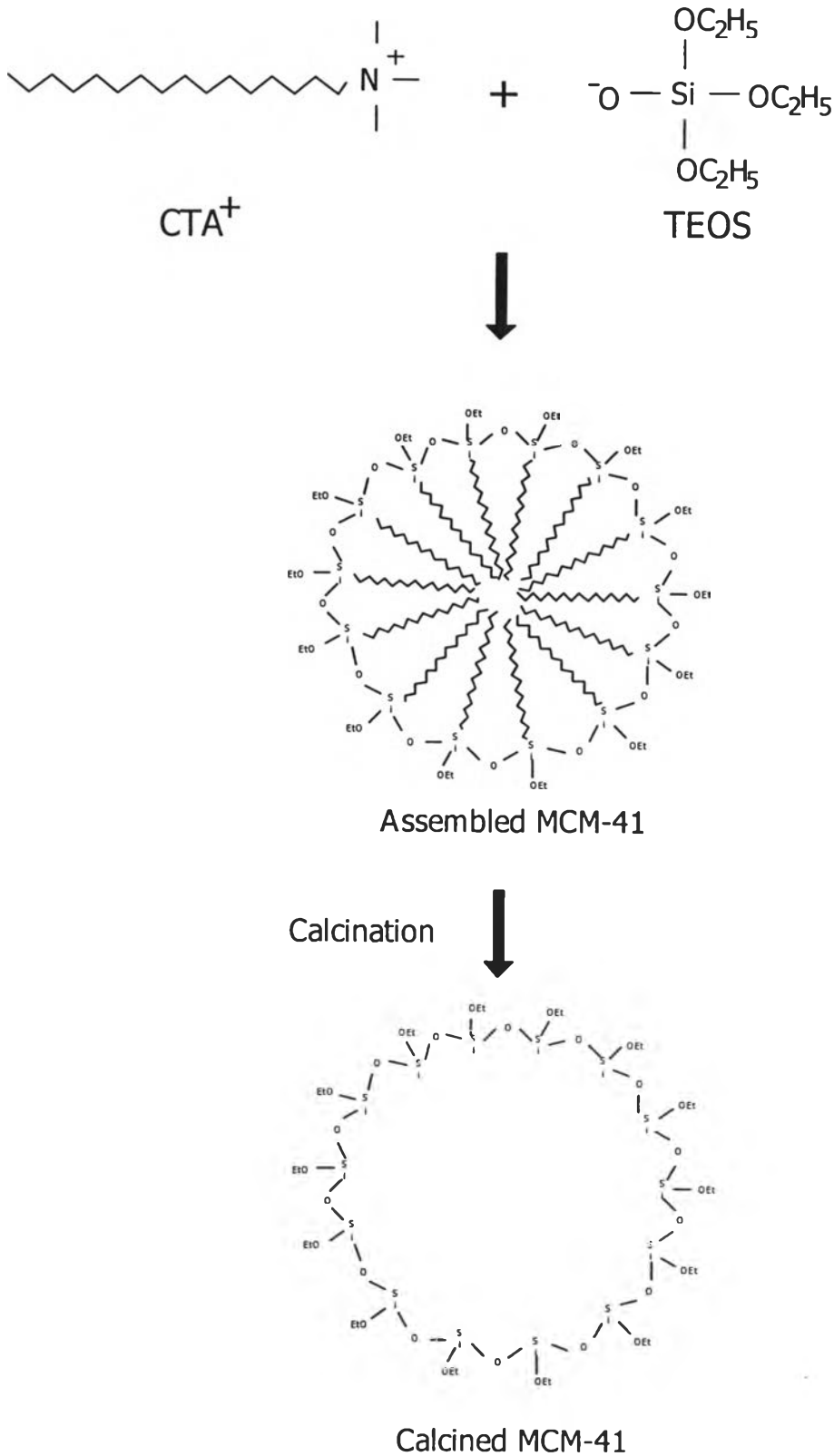

Figure 3-17 Proposed formation of MCM-41 synthesized from CTAB and TEOS; cross-sectional pattern of cylindrical micelles of a silicate complex.

3.5 Summary

Siliceous MCM-41 material synthesized by following the Kumar method showed the unique characteristics of highly ordered MCM-41 as found in many publications. The results from the XRD and FTIR characterizations performed distinctive characteristics of siliceous MCM-41, which are in good agreement with that of other authors. The nitrogen adsorption isotherm was type IVc with a narrow pore size distribution in the range of 20-35 Å. The average pore diameter determined from the BJH model was 29.5 Å and the BET surface area was approximately (800 ± 25) $m^2 g^{-1}$. It was concluded that the synthesized mesoporous sample is the MCM-41 type material with its excellent porous properties. This synthesized MCM-41 was used as the prototype for the synthesis of MCM-41 from rice husk silica (RH-MCM-41) as presented in the next chapter.